

# New Observables in Break-up Reactions of Three-body Halos.

E. Garrido, D.V. Fedorov and A.S. Jensen  
Institute of Physics and Astronomy,  
Aarhus University, DK-8000 Aarhus C, Denmark  
(November 13, 2018)

Momentum distributions of particles from fast three-body halo fragmentation reactions with polarized beams and outgoing fragments are analyzed by use of the sudden approximation. The final state interaction between the two non-disturbed particles is considered. We first give a general and detailed description of the method. We introduce observable quantities that emphasize the two-body correlations in the initial three-body structure as well as in the final two-body system. Using neutron removal from  $^{11}\text{Li}$  as an example we investigate the dependence of the polarization observables on the properties of the low-lying resonances and virtual states of the  $^{10}\text{Li}$  subsystem. These observables are very sensitive to the  $\ell > 0$ -waves in the wave functions, and they provide detailed information on the resonance structure of the neutron-core subsystem.

*PACS:* 25.60.Gc, 25.60.-t, 24.70.+s, 21.45.+v

## I. INTRODUCTION

Halo nuclei have been extensively investigated in the latest years both from the theoretical and experimental point of view. For a review see for instance [1–3] and references therein.

The general properties of light nuclear halos have successfully been revealed by means of few-body models, dividing the degrees of freedom into the approximately frozen (core) and active (halo). Special attention has been paid to three-body Borromean bound systems [4–6], where none of the two-body subsystems is bound. The most prominent examples are  $^6\text{He}$  ( $^4\text{He}+n+n$ ) and  $^{11}\text{Li}$  ( $^9\text{Li}+n+n$ ) both extensively discussed in a general theoretical framework [1].

The most detailed source of experimental information about the structure of these nuclei is the momentum distributions of the particles resulting from the fragmentation reactions [7–13]. For one particle removal reaction with a high energy beam we can consider that the removed particle in the halo projectile is instantaneously captured by the target without disturbing the remaining two. This reaction picture is known as sudden approximation, and has been proved to be fairly accurate in the description of such halo fragmentation reactions [14–19]. For a correct interpretation of the experimental data it is essential to include the interaction between the two non-disturbed particles after the fragmentation, especially when low-lying resonances are present [11,15,18]. Detailed and consistent incorporation of this Final State Interaction (FSI) into the model is necessary as seen by its influence on the momentum distributions [19]. Neutron momentum distributions are very much affected by the final state interaction, but also core momentum distributions are significantly influenced.

A polarized beam interacting with a target is not equally sensitive to all the components of the wave function. It is then possible by means of this tool to observe signals of the less dominant components, and in this way to investigate finer details of the nuclear structure of the projectile. The purpose of this paper is to investigate the effects of polarized beams in fragmentation reactions of fast three-body borromean halo nuclei. The case where the spin projection of one of the particles is measured in the final state will also be considered. We introduce several useful observables and show the kind of information we can extract from them. In particular we consider neutron removal from the polarized  $^{11}\text{Li}$  projectile. The resulting neutron momentum distributions are sensitive to the amount of  $p$ -state admixture in the neutron-core relative state.

The correct description of the structure and reactions of three-body halo nuclei is an indispensable prerequisite for the present investigation. These general procedures are discussed in previous papers [6,20–22] which we shall use extensively. This paper is organized as follows: In section II we formulate the theoretical model and the method used to describe the fragmentation reaction including definition of the polarization observables. The numerical results obtained for  $^{11}\text{Li}$  are reported in section III and in section IV we give a summary and the conclusions. We collect the rather complicated analytic expressions of the differential momentum distributions for different reactions in appendices A and B.

## II. METHOD

The fragmentation reaction is described in the sudden approximation, which assumes that one of the three particles in the projectile is instantaneously removed by the target without disturbing the remaining two. This approximation is valid for a high-energy three-body halo beam interacting with a small target through short range interactions. Therefore we assume a light target where the Coulomb dissociation process only contributes marginally.

The transition matrix in the sudden approximation is given as

$$M = \langle \Phi | \Psi \rangle, \quad (1)$$

where  $\Phi$  is the final state wave function after break-up and  $\Psi$  is the initial wave function of the three-body projectile. We now must specify these wave functions, compute the matrix element and integrate  $|M|^2$  over all the non observed variables.

### A. Wave functions

The initial wave function describes the bound three-body halo system whereas the final state wave function describes the two-body continuum state specified by the experimental conditions.

#### 1. Initial wave function

The projectile three-body wave function  $\Psi$  with inclusion of the proper quantum numbers and variables is denoted by  $\Psi^{JM}(\mathbf{x}, \mathbf{y})$ , where  $J$  and  $M$  are the total spin and its projection. The coordinates  $\mathbf{x}$  and  $\mathbf{y}$  are the usual Jacobi coordinates [20], where  $\mathbf{x}$  is drawn between the two particles surviving after the fragmentation. The wave function is expanded in terms of a complete set of hyperspherical harmonics  $\mathbf{Y}_{\ell_x \ell_y}^{KL}(\alpha, \Omega_x, \Omega_y)$ , where the quantum number  $K$  usually is called the hypermoment,  $\ell_x$  and  $\ell_y$  are the orbital angular momenta associated with  $\mathbf{x}$  and  $\mathbf{y}$ , and  $L$  is resulting from the coupling of these angular momenta. The variables  $\rho$ ,  $\alpha$ ,  $\Omega_x$ , and  $\Omega_y$  are the hyperspherical variables obtained from the Jacobi coordinates  $\mathbf{x}$  and  $\mathbf{y}$  [6]. Then  $\Psi^{JM}(\mathbf{x}, \mathbf{y})$  is written as

$$\Psi^{JM}(\mathbf{x}, \mathbf{y}) = \frac{1}{\rho^{5/2}} \sum_n f_n(\rho) \sum_{K \ell_x \ell_y L s_x S} C_{nK \ell_x \ell_y L s_x S}(\rho) \left[ \mathbf{Y}_{\ell_x \ell_y}^{KL}(\alpha, \Omega_x, \Omega_y) \otimes \chi_{s_x s_y}^S \right]^{JM}, \quad (2)$$

where the spin function  $\chi_{s_x s_y}^S$  is obtained by coupling the spins of two of the particles to  $s_x$  which in turn is coupled to the spin  $s_y$  of the third particle resulting in the total spin  $S$ . The radial functions  $f_n(\rho)$  and the expansion coefficients  $C_{nK \ell_x \ell_y L s_x S}(\rho)$  are calculated numerically by solving the Faddeev equations in coordinate space [20]. Details about this procedure can be found in [20].

#### 2. Final state wave function

The final state wave function  $\Phi$  in the plane wave approximation in the center of mass frame of the projectile is given by

$$\Phi = e^{i\mathbf{k} \cdot \mathbf{R}} \chi_{s_y}^{\sigma_y} e^{i\mathbf{q} \cdot \mathbf{r}} \chi_{s_1}^{\sigma_1} \chi_{s_2}^{\sigma_2}, \quad (3)$$

where  $\chi_{s_i}^{\sigma_i}$  for  $i=1,2$  and  $\chi_{s_y}^{\sigma_y}$  are the spin wave functions respectively for the two undisturbed particles and the third removed particle. Here  $s$  and  $\sigma$  are the total spin and its projection on an axis. Furthermore  $\mathbf{k}$  and  $\mathbf{q}$  are the total and relative momentum of the two remaining particles in the final state,  $\mathbf{r}$  is the distance between the two remaining particles, and  $\mathbf{R}$  is the distance between the center of mass of this two-body system and the removed particle.

The description in terms of plane waves in Eq.(3) implies that all the interactions between the particles are neglected in the final state wave function. However, in our approximation only one of the particles is removed from the other two, and the interaction between the non-disturbed particles can not be neglected. In a recent work [19] we investigated the influence of this final state interaction (FSI) on the momentum distributions, and observed that they are crucial for reproduction of the experimental momentum distributions.

In Eq.(3) introduction of the final state interaction amounts to substitution of the plane wave,  $e^{i\mathbf{q}\cdot\mathbf{r}}\chi_{s_1}^{\sigma_1}\chi_{s_2}^{\sigma_2}$ , describing the two-body system in the final state by the appropriate *distorted* two-body wave function  $w$ . When the two-body interaction do not mix the two-body states with different spin  $s_x$  and relative orbital angular momentum  $\ell_x$ , we can expand this two-body wave function ( $w$ ) in partial waves as in [23]. These assumptions are usually strictly valid. The only exception arises from the tensor interaction. However the resulting mixing is often very small and therefore insignificant in the present context. We then have

$$w^{\sigma_1\sigma_2}(\mathbf{k}_x, \mathbf{x}) = \sum_{s_x\sigma_x} \langle s_1\sigma_1 s_2\sigma_2 | s_x\sigma_x \rangle w^{s_x\sigma_x}(\mathbf{k}_x, \mathbf{x}), \quad (4)$$

with

$$w^{s_x\sigma_x}(\mathbf{k}_x, \mathbf{x}) = \sqrt{\frac{2}{\pi}} \frac{1}{k_x x} \sum_{j_x \ell_x m_x} u_{\ell_x s_x}^{j_x}(k_x, x) \mathcal{Y}_{j_x \ell_x s_x}^{m_x*}(\Omega_x) \\ \times \sum_{m_{\ell_x}=-\ell_x}^{\ell_x} \langle \ell_x m_{\ell_x} s_x \sigma_x | j_x m_x \rangle i^{\ell_x} Y_{\ell_x m_{\ell_x}}(\Omega_{k_x}), \quad (5)$$

where  $\mathbf{k}_x$  is the momentum associated with  $\mathbf{x}$ ,  $\sigma_x$  is the spin projection of  $s_x$ ,  $u$  is the radial and  $\mathcal{Y}$  the angular distorted wave function. The angles  $\Omega_x$  and  $\Omega_{k_x}$  define the direction of  $\mathbf{x}$  and  $\mathbf{k}_x$ , respectively. The dependence on the spins  $s_1$  and  $s_2$  of the two particles surviving after the fragmentation reaction has been omitted for notational simplicity.

The radial wave functions  $u_{\ell_x s_x}^{j_x}(k_x, x)$  are obtained numerically by solving the Schrödinger equation with the appropriate two-body potential  $\hat{V}(\mathbf{x})$

$$\frac{\partial^2}{\partial x^2} u_{\ell_x s_x}^{j_x}(k_x, x) + \left( k_x^2 - \frac{2m}{\hbar^2} V_{\ell_x s_x}^{j_x}(x) - \frac{\ell_x(\ell_x + 1)}{x^2} \right) u_{\ell_x s_x}^{j_x}(k_x, x) = 0, \quad (6)$$

where the effective radial potential is obtained by integration over the angles  $\Omega_x$

$$V_{\ell_x s_x}^{j_x}(x) = \int d\Omega_x \mathcal{Y}_{j_x \ell_x s_x}^{m_x*}(\Omega_x) \hat{V}(\mathbf{x}) \mathcal{Y}_{j_x \ell_x s_x}^{m_x}(\Omega_x) \quad (7)$$

and  $m$  is an arbitrary normalization mass.

## B. Transition matrix element

The calculation of the transition matrix requires now the overlap of the initial three-body wave function in Eq.(2) and the final state wave function  $e^{i\mathbf{k}\cdot\mathbf{R}}\chi_{s_y}^{\sigma_y} w^{\sigma_1\sigma_2}(\mathbf{k}_x, \mathbf{x})$ , where  $\mathbf{k}_y$  is the momentum associated with the  $\mathbf{y}$  coordinate. Since  $\mathbf{k}_y \cdot \mathbf{y} = \mathbf{k} \cdot \mathbf{R}$  we then find

$$M_{\sigma_1\sigma_2\sigma_y}^{JM}(\mathbf{k}_x, \mathbf{k}_y) = \sum_{s_x\sigma_x} \langle s_1\sigma_1 s_2\sigma_2 | s_x\sigma_x \rangle M_{s_x\sigma_x s_y\sigma_y}^{JM}(\mathbf{k}_x, \mathbf{k}_y) \quad (8)$$

For simplicity we do not specify the dependence of  $M_{\sigma_1\sigma_2\sigma_y}^{JM}(\mathbf{k}_x, \mathbf{k}_y)$  on the spins  $s_1$ ,  $s_2$  and  $s_y$  of the three particles involved in the reaction.

The analytic form of  $M_{s_x\sigma_x s_y\sigma_y}^{JM}(\mathbf{k}_x, \mathbf{k}_y)$  is

$$M_{s_x\sigma_x s_y\sigma_y}^{JM}(\mathbf{k}_x, \mathbf{k}_y) \propto \frac{2}{\pi} \sum_{\ell_x m_{\ell_x} \ell_y m_{\ell_y}} \sum_{j_x LS} I_{\ell_x s_x j_x}^{\ell_y LS}(\kappa, \alpha_\kappa) Y_{\ell_x m_{\ell_x}}(\Omega_{k_x}) Y_{\ell_y m_{\ell_y}}(\Omega_{k_y}) \\ \times \sum_{m_x j_y m_y} (-1)^{J+2S-2M+\ell_y+s_y-s_x-\ell_x} \hat{j}_x \hat{j}_y \hat{J} \hat{L} \hat{S} \begin{pmatrix} J & j_x & j_y \\ M & -m_x & -m_y \end{pmatrix} \\ \times \begin{pmatrix} j_y & \ell_y & s_y \\ -m_y & m_{\ell_y} & \sigma_y \end{pmatrix} \begin{pmatrix} j_x & \ell_x & s_x \\ -m_x & m_{\ell_x} & \sigma_x \end{pmatrix} \begin{Bmatrix} J & j_x & j_y \\ L & \ell_x & \ell_y \\ S & s_x & s_y \end{Bmatrix} \quad (9)$$

where  $\hat{a} = \sqrt{2a+1}$ . In Eq.(9) we have introduced the hyperspherical coordinates in momentum space  $\kappa = \sqrt{k_x^2 + k_y^2}$ ,  $\alpha_\kappa = \arctan(k_x/k_y)$ , and the numerical function  $I_{\ell_x s_x j_x}^{\ell_y L S}(\kappa, \alpha_\kappa)$  is given by

$$I_{\ell_x s_x j_x}^{\ell_y L S}(\kappa, \alpha_\kappa) = i^{\ell_x + \ell_y} \sum_{Kn} N_K^{\ell_x \ell_y} \int \rho^{5/2} d\rho f_n(\rho) C_{nK\ell_x \ell_y L s_x S}(\rho) \left[ \int d\alpha (\sin \alpha)^{\ell_x + 2} (\cos \alpha)^{\ell_y + 2} P_\nu^{\ell_x + \frac{1}{2}, \ell_y + \frac{1}{2}}(\cos(2\alpha)) j_{\ell_y}(k_y y) u_{\ell_x s_x}^{j_x}(k_x, x) \right] \quad (10)$$

where  $\nu = (K - \ell_x - \ell_y)/2$ ,  $P_\nu^{\ell_x + \frac{1}{2}, \ell_y + \frac{1}{2}}$  is a Jacobi polynomial, and

$$N_K^{\ell_x \ell_y} = \left[ \frac{\nu!(\nu + \ell_x + \ell_y + 1)!2(K+2)}{\Gamma(\nu + \ell_x + \frac{3}{2})\Gamma(\nu + \ell_y + \frac{3}{2})} \right]^{1/2}. \quad (11)$$

### C. Cross sections

The cross section or momentum distribution is now obtained by squaring the transition matrix, and subsequently averaging over initial states and summing up over final states. If we consider the possibility of having a polarized beam and measuring the spin projection of the two particles in the final state we can then write

$$\frac{d^6\sigma}{d\mathbf{k}_x d\mathbf{k}_y} \propto \sum_M W_{\text{init.}}(M) \sum_{\sigma_1} W_{\text{fin.}}(\sigma_1) \sum_{\sigma_2} W_{\text{fin.}}(\sigma_2) \sum_{\sigma_y} |M_{\sigma_1 \sigma_2 \sigma_y}^{JM}(\mathbf{k}_x, \mathbf{k}_y)|^2 \quad (12)$$

where  $W_{\text{init.}}(M)$ ,  $W_{\text{fin.}}(\sigma_1)$ , and  $W_{\text{fin.}}(\sigma_2)$  give the occupation probability of each magnetic substate in the initial and final states. When the beam is unpolarized and there is no detection of final spin projections these probabilities take the values  $W_{\text{fin.}}(M) = 1/(2J+1)$ ,  $W_{\text{fin.}}(\sigma_1) = 1/(2s_1+1)$ , and  $W_{\text{fin.}}(\sigma_2) = 1/(2s_2+1)$ , and we obtain the unpolarized expression for the momentum distributions [19].

The volume element  $d\mathbf{k}_x d\mathbf{k}_y$  is written

$$d\mathbf{k}_x d\mathbf{k}_y = k_x^\perp dk_x^\perp dk_x^\parallel d\varphi_{k_x} k_y^2 dk_y d\Omega_{k_y} \quad (13)$$

where  $k_x^\perp = k_x \sin \theta_{k_x}$ ,  $k_x^\parallel = k_x \cos \theta_{k_x}$ , and  $(\theta_{k_x}, \varphi_{k_x})$  are the polar and azimuthal angles associated to  $\Omega_{k_x}$ .

The integration of Eq.(12) over  $\Omega_{k_y}$  and  $\varphi_{k_x}$  can be done analytically. By further numerical integration over  $k_y$  and  $k_x^\perp$ , we get the one-dimensional relative momentum ( $k_x^\parallel$ ) distribution of the remaining particles. By integrating over  $k_y$  and  $k_x^\parallel$ , we get instead the two-dimensional relative momentum ( $k_x^\perp$ ) distribution. It should be noted that we have not specified any coordinate system and the axes  $\mathbf{x}$ ,  $\mathbf{y}$ , and  $\mathbf{z}$  are therefore completely arbitrary. Thus, in the sudden approximation the longitudinal and transverse momentum distributions are identical.

After substituting Eqs.(8) and (9) into (12), and integrating analytically over  $\Omega_{k_y}$  and  $\varphi_{k_x}$  we obtain the expressions for the three-differential momentum distributions that are collected in appendix A. Three different cases are considered:

(i) Eq.(A1) describes the process with 100% polarized beam where the polarization of one of the particles in the final state is measured, i.e.  $W_{\text{init.}}(M') = \delta_{MM'}$ ,  $W_{\text{fin.}}(\sigma'_1) = \delta_{\sigma_1 \sigma'_1}$ ,  $W_{\text{fin.}}(\sigma'_2) = 1/(2s_2+1)$ ,

(ii) Eq.(A2) describes the process with 100% polarized beam without detection of the final spin states, i.e.  $W_{\text{init.}}(M') = \delta_{MM'}$ ,  $W_{\text{fin.}}(\sigma'_1) = 1/(2s_1+1)$ ,  $W_{\text{fin.}}(\sigma'_2) = 1/(2s_2+1)$ ,

(iii) Eq.(A3) describes the process with unpolarized beam without detection of the final spin states, i.e.  $W_{\text{init.}}(M') = 1/(2J+1)$ ,  $W_{\text{fin.}}(\sigma'_1) = 1/(2s_1+1)$ ,  $W_{\text{fin.}}(\sigma'_2) = 1/(2s_2+1)$ .

To compare with the experimental data the momentum distributions should be referred to the center of mass frame of the projectile. To do this we construct the momentum  $\mathbf{p}$  of one of the particles in the final state relative to the center of mass of the projectile as a linear combination of  $\mathbf{k}_x$  and  $\mathbf{k}_y$ , i.e.

$$\mathbf{p} = a_i \mathbf{k}_x + b_i \mathbf{k}_y, \quad (14)$$

where  $i = 1, 2$  refer to the two remaining particles. If the Jacobi coordinate  $\mathbf{x}$  goes from particle 1 to particle 2, then  $a$  and  $b$  take the values

$$a_1 = - \left( \frac{1}{m} \frac{m_1 m_2}{m_1 + m_2} \right)^{1/2}, \quad b_1 = \frac{m_1}{m_1 + m_2} \left( \frac{1}{m} \frac{(m_1 + m_2) m_3}{m_1 + m_2 + m_3} \right)^{1/2}, \quad (15)$$

$$a_2 = \left( \frac{1}{m} \frac{m_1 m_2}{m_1 + m_2} \right)^{1/2}, \quad b_2 = \frac{m_2}{m_1 + m_2} \left( \frac{1}{m} \frac{(m_1 + m_2) m_3}{m_1 + m_2 + m_3} \right)^{1/2}, \quad (16)$$

when we compute the momentum distributions of particle 1 and 2, respectively.

Since the volume element  $d\mathbf{p}d\mathbf{k}_y = a_i^3 d\mathbf{k}_x d\mathbf{k}_y$  we obtain the relation

$$\frac{d^6\sigma}{d\mathbf{p}d\mathbf{k}_y} = \frac{1}{a_i^3} \frac{d^6\sigma}{d\mathbf{k}_x d\mathbf{k}_y}. \quad (17)$$

The only additional complication in this coordinate system is that the numerical function  $I_{\ell_x s_x j_x}^{\ell_y L S}(\kappa, \alpha_\kappa)$  now depends on the relative angle  $\theta'_{\mathbf{k}_y}$  between  $\mathbf{p}$  and  $\mathbf{k}_y$ . Only two angular integrations can then be performed analytically, and three integrations must be done numerically in order to get the one-dimensional and two-dimensional momentum distributions of one of the particles in the final state relative to the center of mass of the projectile.

In appendix B we show the analytic expressions for the four-differential momentum distributions relative to the center of mass of the projectile for the same three cases as specified in appendix A. They are given by Eqs.(B1), (B2) and (B3), respectively.

#### D. Polarization Observables

We shall denote the one and two-dimensional momentum distributions when the beam is unpolarized and the spin projection of the particles is not measured in the final state by  $\mathcal{Q}_1(p^\parallel) = d\sigma/dp^\parallel$  and  $\mathcal{Q}_2(p^\perp) = d\sigma/dp^\perp$ , respectively. The distributions are referred to the center of mass of the three-body projectile, and obtained by integration over the unobserved quantities of Eq.(B3) in appendix B.

In the same way we shall denote the one and two-dimensional momentum distributions when the beam is 100% polarized (with spin projection  $M$ ) and the spin projection of the particles in the final state is not measured by  $\mathcal{Q}_1^M(p^\parallel) = d\sigma^M/dp^\parallel$  and  $\mathcal{Q}_2^M(p^\perp) = d\sigma^M/dp^\perp$ , respectively. These distributions are obtained by integration of Eqs.(B2) in appendix B.

Finally,  $\mathcal{Q}_1^{M\sigma}(p^\parallel) = d\sigma^{M\sigma}/dp^\parallel$  and  $\mathcal{Q}_2^{M\sigma}(p^\perp) = d\sigma^{M\sigma}/dp^\perp$  will denote the one and two-dimensional momentum distributions for a 100% polarized beam (with spin projection  $M$ ), and when the spin projection of one of the particles in the final state is measured to be  $\sigma$ . These distributions are obtained by integration of Eqs.(B1) in appendix B.

We define now the following asymmetries

$$A_i^{MM'} \equiv \frac{\mathcal{Q}_i^M - \mathcal{Q}_i^{M'}}{\mathcal{Q}_i}, \quad i = 1, 2 \quad (18)$$

$$A_i^{MM';\sigma\sigma'} \equiv \frac{\mathcal{Q}_i^{M\sigma} - \mathcal{Q}_i^{M'\sigma'}}{\mathcal{Q}_i}, \quad i = 1, 2 \quad (19)$$

It is easy to check that the  $I = I' = 0$  term in Eq.(B1) and the  $I = 0$  term in Eq.(B2) are independent of  $M$  and  $\sigma$ , and equal to the totally unpolarized momentum distribution Eq.(B3). This means that the deviations from zero of the asymmetries Eqs.(18) and (19) are a direct consequence of the polarization of the beam and the measure of the spin projection of one of the particles after the fragmentation.

Direct examination of Eq.(B2) permits us to observe that if only  $s$ -waves were involved in the initial and final wave functions ( $\ell_x = \ell'_x = L_x = 0$  and  $\ell_y = \ell'_y = L_y = 0$ ) only the  $I=0$  term would contribute to the momentum distribution. In other words, the asymmetry Eq.(18) would vanish. Therefore, the deviation from zero of this asymmetry is a signal of non-vanishing components different from  $s$ -waves in the wave function. This conclusion is not true for the asymmetry Eq.(19), since the momentum distribution Eq.(B1) has additional non-vanishing terms even when only  $s$ -waves are involved.

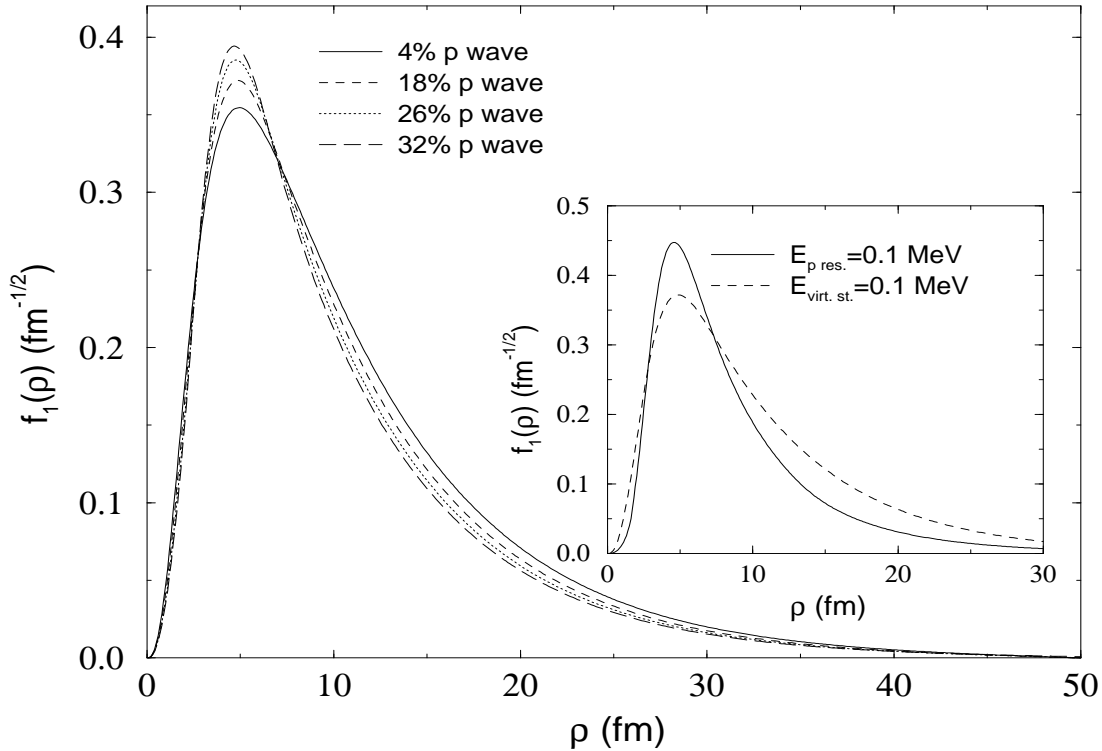


FIG. 1. The radial wave function  $f_1(\rho)$  for  $^{11}\text{Li}$  when  $^{10}\text{Li}$  has a virtual  $s$ -state at 100 keV the lowest-lying  $p$ -resonance at 0.5 MeV. Calculations with 4% of  $p$ -wave (solid line), 18% of  $p$ -wave (short-dashed line), 26% of  $p$ -wave (dotted line), and 32% (long-dashed line) in the  $^{10}\text{Li}$  wave function are shown. The inset shows the same wave function when  $^{10}\text{Li}$  has a low-lying virtual  $s$ -state at 100 keV (dashed line) and when  $^{10}\text{Li}$  has a low-lying  $p$ -resonance at 100 keV (solid line).

### III. RESULTS

In this section we apply the procedure described above to two-neutron halo nuclei, and in particular to  $^{11}\text{Li}$ . We consider neutron removal reactions, and the neutron- $^9\text{Li}$  interaction is include in the final state. We only included  $s$ - and  $p$ -waves in the calculations, since components with higher angular momenta are negligibly small. We use the two-body potentials described in ref. [21], i.e.

$$V_{nn} = \left( V_c + V_{ss} \mathbf{s}_{n1} \cdot \mathbf{s}_{n2} + V_T \hat{S}_{12} + V_{so} \mathbf{l}_{nn} \cdot \mathbf{s}_{nn} \right) \exp \left[ -(r/b_{nn})^2 \right] \quad (20)$$

$$V_{nc}^{(s)} = V_s (1 + \gamma_s \mathbf{s}_c \cdot \mathbf{s}_n) \exp \left[ -(r/b_{nc})^2 \right], \quad (21)$$

$$V_{nc}^{(l)} = (V_l + V_{so}^{(l)} \mathbf{l}_{nc} \cdot \mathbf{s}_{nc}) \exp \left[ -(r/b_{nc})^2 \right], \quad (22)$$

The nucleon-nucleon potential  $V_{nn}$  is made of gaussians containing central ( $V_c$ ), spin splitting ( $V_{ss}$ ), spin-orbit ( $V_{so}$ ) and tensor ( $V_T$ ) parts where the parameters are fitted to low energy  $s$ - and  $p$ -wave nucleon-nucleon scattering data ( $\mathbf{s}_{n1}$  and  $\mathbf{s}_{n2}$  are the spins of the two neutrons,  $\mathbf{l}_{nn}$  is the two-neutron relative orbital angular momentum,  $\mathbf{s}_{nn} = \mathbf{s}_{n1} + \mathbf{s}_{n2}$ , and  $\hat{S}_{12}$  is the usual tensor operator). In the neutron-neutron subsystem more than 98% of the probability is found in  $s$ -waves.

The neutron-core potential  $V_{nc}$  is also made of gaussians adjusted to reproduce the experimental binding energy and root mean square radius of the three-body projectile ( $295 \pm 35$  keV [24] and  $3.1 \pm 0.3$  fm [25], respectively, for  $^{11}\text{Li}$ ). The different waves are independently fitted, allowing us to adjust separately the energy positions of the virtual  $s$ -states and the resonances in the neutron-core subsystem. For simplicity the spin splitting term (introduced by the parameter  $\gamma_s$ ) has been included only for  $s$ -waves in the neutron-core interaction.

### A. Initial and final wave functions

The expression we use for the wave function of the three-body halo projectile is given by Eq.(2), where the radial functions  $f_n(\rho)$  and the coefficients  $C_{nK\ell_x\ell_yLs_xS}(\rho)$  are computed numerically. To illustrate some of the general aspects of the three-body wave functions, we show in Fig. 1 the  $f_1(\rho)$  function for  $^{11}\text{Li}$ . This function dominates the expansion in Eq.(2) as it contains more than 95% of the norm of the total wave function. The neutron-core interaction has been fitted to produce a low-lying virtual  $s$ -state at 100 keV and the lowest  $p$ -resonance at 0.5 MeV. By use of the spin-orbit parameter ( $V_{so}^{(l=1)}$ ) we can move the higher-lying  $p$ -resonances up or down and thereby modify the  $p$ -wave content in the neutron- $^9\text{Li}$  subsystem. Four different situations of varying  $p$ -wave content are shown, i.e. 4% (solid line), 18% (short-dashed line), 26% (dotted line) and 32% (long-dashed line). We observe that the more  $p$ -wave content in the neutron- $^9\text{Li}$  subsystem the narrower the radial wave function. This result can be attributed to the centrifugal barrier, that keeps the neutrons closer to the core for  $p$ -waves.

When the final state interaction is neglected in the calculation, the momentum distributions are given by the square of the Fourier transform of the three-body wave function in Eq.(2). Therefore a larger  $p$ -wave content in the neutron-core subsystem will produce a broader momentum distribution. Details about calculations of momentum distributions following this method have been presented in [19]. Nevertheless, the differences between the three-body wave functions in Fig. 1 are not very large and the corresponding momentum distributions would also be very similar. In the inset of Fig. 1 we display the same radial three-body wave function  $f_1(\rho)$  for a neutron-core potential producing a  $p$ -resonance at 100 keV (solid line) and a virtual  $s$ -state at 100 keV (dashed line). Again we find that the low-lying  $p$ -resonance produces a narrower radial wave function, and therefore a broader momentum distribution (without FSI). In this case the difference between the wave functions is larger and as a consequence the momentum distributions for a low-lying  $p$ -resonance and a low-lying virtual  $s$ -state will also be clearly distinguishable.

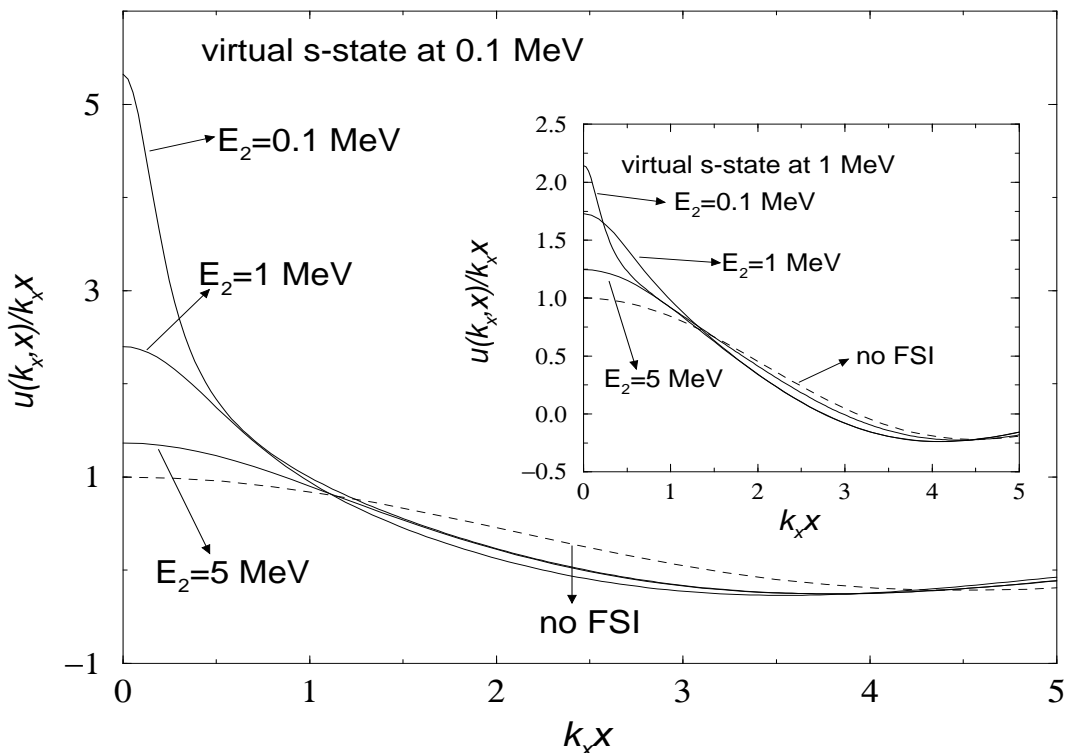


FIG. 2. Continuum radial  $s$ -state wave functions in Eq.(4) when the neutron- $^9\text{Li}$  system has a virtual  $s$ -state at 0.1 MeV. Three different two-body scattering energies ( $E_2 = \hbar^2 k_x^2 / 2m$ ) are considered, 0.1 MeV, 1 MeV and 5 MeV. The dashed line is the same wave function when the neutron- $^9\text{Li}$  interaction is neglected. The inset show the same wave function when the neutron- $^9\text{Li}$  subsystem has a virtual  $s$ -state at 1 MeV.

To analyze the effect of the inclusion of the final state interaction we investigate the behaviour of the distorted wave function in Eq.(4). First we consider a neutron-core potential with a virtual  $s$ -state at 100 keV, and investigate how the corresponding continuum radial  $s$ -state wave functions behave for different energies  $E_2 (= k_x^2 \hbar^2 / 2m)$  of the

neutron-core system. When the final state interaction is neglected this radial  $s$ -state wave function is simply the Bessel function  $j_0(k_x x)$ , which in Fig. 2 (the dashed line) is compared to the distorted wave functions (the solid lines) for different values of  $E_2=0.1$  MeV, 1 MeV and 5 MeV. At large distances (not shown in the figure) the oscillations continue and have the same amplitude.

The difference from the Bessel function is only significant at small distance and this difference increases in general when  $E_2$  approaches the energy of the virtual state. (Note, however, the singularity at the origin for vanishing  $E_2$ .) Therefore for small values of  $k_x$  the overlap in Eq.(1) is larger than in Eq.(8) and since the normalization is the same in all cases, the momentum distribution becomes narrower by inclusion of final state interactions.

The inset in Fig. 2 shows the same plot as in the main part, but for a neutron-core potential with a virtual  $s$ -state at 1 MeV. The general conclusions are the same, the smaller  $E_2$  the larger the effect of the final state interaction. However, in this case the difference with the Bessel function is clearly smaller (note the different vertical scales), and therefore also the influence of the final state interaction is smaller. We can then conclude that the inclusion of final state interaction in  $s$ -waves makes the momentum distribution narrower, and the smaller the energy of the virtual  $s$ -state the larger the effect of the final state interaction.

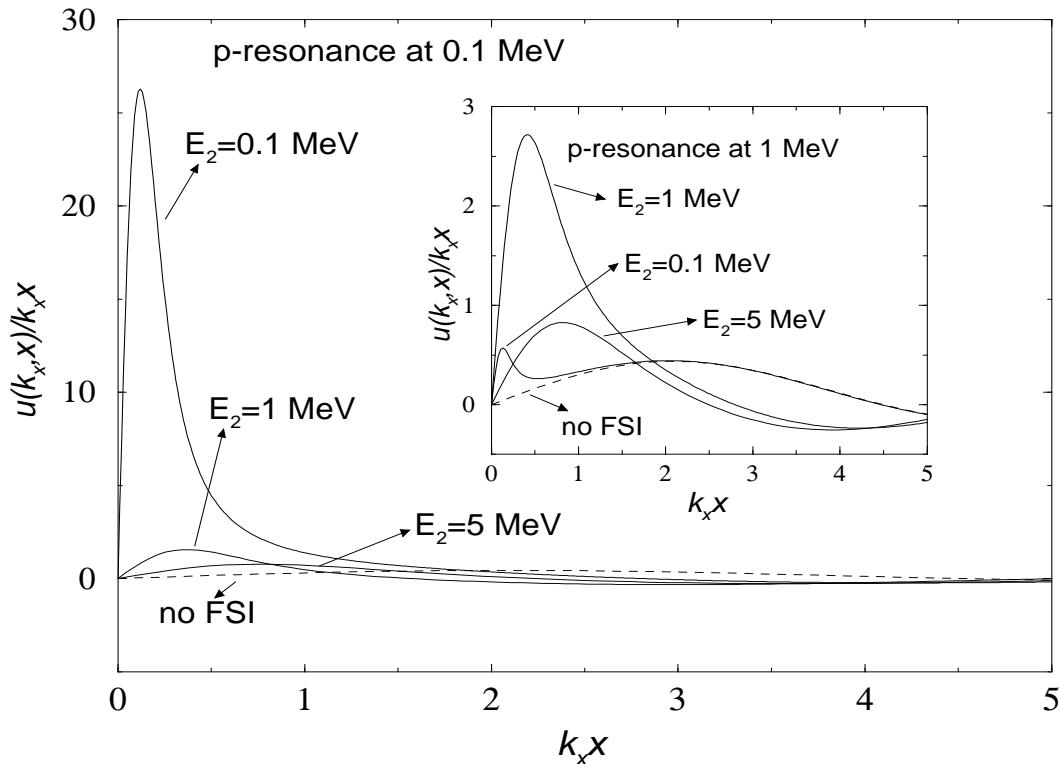


FIG. 3. The same as Fig. 2 for  $p$ -resonances instead of virtual  $s$ -states.

In Fig. 3 we show the same quantities as in Fig. 2, but now for  $p$ -waves. In the main part of the figure we consider a neutron-core potential with a  $p$ -resonance at 0.1 MeV. Again the dashed line is the radial part of the  $p$ -wave without final state interaction (equal to the Bessel function  $j_1(k_x x)$ ). When we solve the Schrödinger equation for a  $p$ -wave and when  $E_2 (= k_x^2 \hbar^2 / 2m)$  is far from the resonance energy (we have taken  $E_2 = 5$  MeV) the difference with the Bessel function is very small, and the effect of the final state interaction is almost negligible. When  $E_2$  approaches the energy of the resonance the  $p$ -wave becomes more and more localized, in such a way that it gets a maximum for  $E_2$  equal to the energy of the resonance (0.1 MeV in this case). As a consequence, the overlap in Eq.(8) is maximum for  $k_x = \sqrt{2mE_{\text{res}}/\hbar^2}$ , and the momentum distributions are enhanced around that value of  $k_x$ .

The inset of Fig. 3 shows the same as in the main part for  $E_{\text{res}} = 1$  MeV. The behaviour of the  $p$ -wave is identical to the previous one. The wave is very much localized and gets its maximum value for  $E_2 = E_{\text{res}}$ . However, the maximum is now clearly smaller than in the previous case of  $E_{\text{res}} = 0.1$  MeV, and therefore also the effect on the momentum distributions is less pronounced. Therefore, the inclusion of the final state interaction in the  $p$ -wave will produce an increase in the momentum distributions around  $k_x = \sqrt{2mE_{\text{res}}/\hbar^2}$ . This increase is especially important when



the neutron-core potential has a low-lying  $p$ -resonance, and again, due to the normalization, makes the momentum distributions narrower.

Summarizing, the inclusion of final state interaction highly modifies the momentum distributions for  $s$ - and  $p$ -waves. This change is clearly more significant for low-lying virtual  $s$ -states and low-lying  $p$ -resonances. For  $s$ -waves the distributions are enhanced at the origin ( $k_x = 0$ ), and for  $p$ -waves the enhancement is produced at  $k_x = \sqrt{2mE_{\text{res}}/\hbar^2}$ . In both cases the momentum distributions become narrower by inclusion of the final state interaction.

Before concluding this subsection we must emphasize that the momentum distributions discussed so far were expressed in terms of  $k_x$ , i.e. the relative momentum between the two remaining particles. From Eqs.(14) - (16) we see that the momentum of the neutron relative to the center of mass of the projectile is very close to  $k_x$  (the  $b$  coefficient is small due to the large mass of the core). Therefore the above conclusions about the effect of the final state interaction roughly remain unchanged for the neutron momentum distributions relative to the center of mass of the projectile.

For the core momentum distribution the  $b_i$  coefficient in Eq.(14) is large, and the effect of the final state interaction is much smaller when we refer momentum distributions of the core to the center of mass of the projectile. The reason is simply that the center of mass of the core is fairly close to the center of mass of the total three-body system.

## B. Asymmetries

Experimental data suggest that the neutron unbound  $^{10}\text{Li}$  system has a  $p$ -resonance around 0.5 MeV [26] and a low-lying ( $\leq 0.2$  MeV) virtual  $s$ -state or  $p$ -resonance [11,26–28]. In all the computations reported in this work the neutron-core potential is fitted to produce a  $p$ -resonance at 0.5 MeV in  $^{10}\text{Li}$ . For the lowest-lying state we investigate several possibilities in order to analyze the dependence of the polarization observables on the properties of the lowest-lying state.

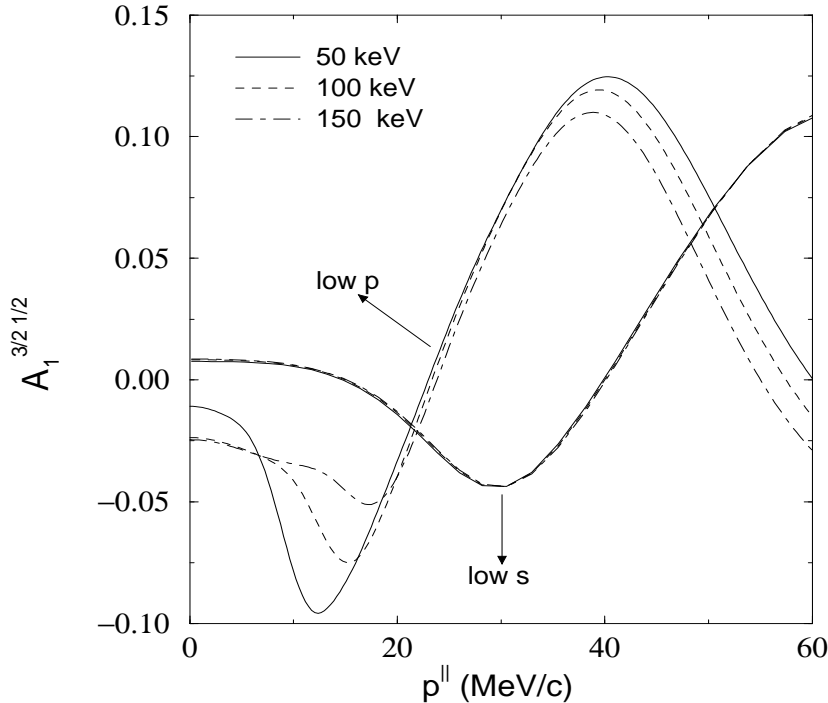


FIG. 4. Asymmetry  $A_1^{3/2 1/2}(p^{\parallel})$  for neutron momentum distributions in a neutron removal  $^{11}\text{Li}$  fragmentation reaction. A low-lying state is assumed in  $^{10}\text{Li}$  at 50 keV (solid line), 100 keV (dashed line) or at 150 keV (dot-dashed line). The cases of low-lying  $p$ -resonances and low-lying virtual  $s$ -states are both shown (see figure).

In Fig. 4 we show the asymmetry  $A_1^{3/2 1/2}(p^{\parallel})$  for neutron momentum distributions after a neutron removal  $^{11}\text{Li}$  fragmentation reaction. A low-lying state ( $s$ - or  $p$ -wave) is present in  $^{10}\text{Li}$  at 50 keV (solid line), 100 keV (dashed

line) or at 150 keV (dot-dashed line). For low-lying  $p$ -resonances we observe for all the three energies two peaks in the asymmetry. The first peak at low momentum corresponds to the lowest-lying  $p$ -resonance. The second peak is in all the three cases generated by the  $p$ -resonance at 0.5 MeV. The connection between the position of the different minima and maxima of the asymmetry and the energy of the  $p$ -resonance may be seen from the relations  $k_x = p_r \sqrt{m/\mu}$  and  $k_x = \sqrt{2mE_{\text{res}}/\hbar^2}$ , where  $p_r$  is the relative neutron-core momentum,  $E_{\text{res}}$  is the energy of the resonance and  $\mu$  is the reduced mass of the neutron-core subsystem. The different  $p$ -resonance energies in the figure correspond to values  $p_r$  of 10 MeV/c, 14 MeV/c, and 17 MeV/c, respectively and an energy of 0.5 MeV corresponds to  $p_r \approx 30$  MeV/c.

As discussed in section 2, the momentum distributions are enhanced around the resonance value of  $k_x$ , that is very close to the momentum of the neutron relative to the center of mass of the three-body projectile. This increase in the momentum distributions produces the oscillations in the asymmetry. As a consequence, when the energy of the resonance increases the peak in the asymmetry is displaced towards higher momenta. Since we plot the asymmetries as functions of the longitudinal component of the neutron momentum relative to the center of mass of the projectile (that is not exactly  $p_r$ , but very close), the maxima and minima of the asymmetry do not exactly coincide with these numbers. However, the connection to the energy of the resonances in the neutron-core subsystem is very clear.

Inspecting the asymmetry in Fig. 4 where a low-lying virtual  $s$ -state is present in  $^{10}\text{Li}$  we observe that the first peak completely disappears. This fact was expected, since in section 2 we showed that the asymmetry Eq.(18) vanishes when only  $s$ -waves are involved in the wave functions. In other words, the asymmetry  $A_1^{3/2\ 1/2}(p^\parallel)$  does not feel the presence of virtual  $s$ -states in the neutron-core subsystem, and it is only sensitive to the structure of the non zero angular momentum resonances. Since only  $s$ -waves are changed for the three different cases considered, the asymmetries are essentially indistinguishable.

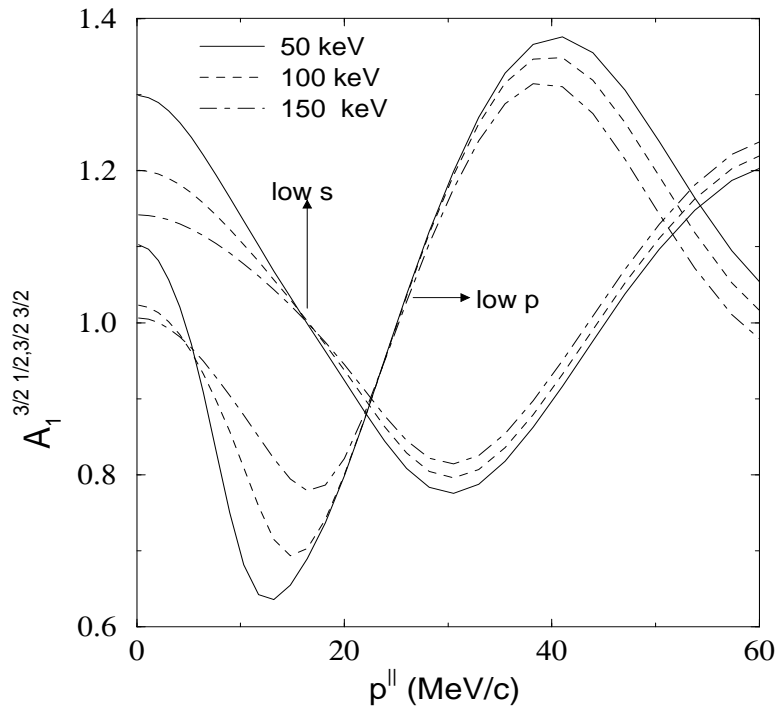


FIG. 5. The same as in Fig. 4 for the asymmetry  $A_1^{3/2\ 1/2;3/2\ 3/2}(p^\parallel)$ .

Let us now consider the case where the spin projection of one of the particles in the final state is measured. In particular we assume that the spin projection of the core is measured to be  $3/2$ , and construct the asymmetry  $A_1^{3/2\ 1/2;3/2\ 3/2}(p^\parallel)$  for neutron momentum distributions in a neutron removal reaction. The result is shown in Fig. 5 for the cases corresponding to Fig. 4. Again, for low-lying  $p$ -resonances there are two peaks in the asymmetry, one of them connected to the energy of the low-lying resonance and the other peak is related to the resonance at 0.5 MeV.

For low-lying virtual  $s$ -states the first peak disappears, and only the peak associated with the  $p$ -resonance at 0.5 MeV remains. Now the  $s$ -waves also contribute to the asymmetry, but the contribution is localized in the region close

to the origin where the curves now are different for the three energies of the low-lying virtual  $s$ -state. Therefore the asymmetries shown in Fig. 5 display the same features as those of Fig. 4. The main difference is that the amplitude of the oscillations of the asymmetries clearly is larger in the asymmetries shown in Fig. 5.

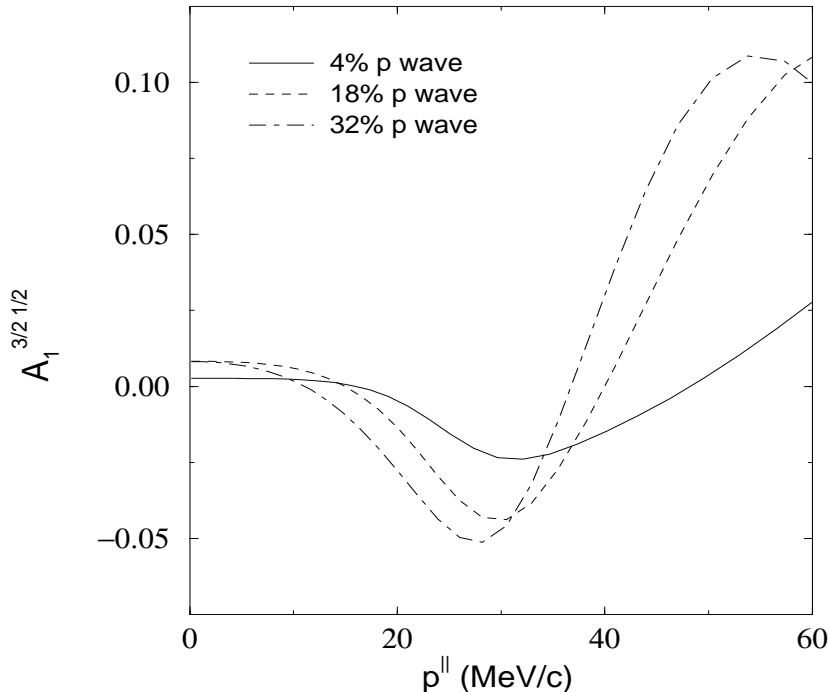


FIG. 6. Asymmetry  $A_1^{3/2, 1/2}(p^{\parallel})$  for neutron momentum distributions in a neutron removal  $^{11}\text{Li}$  fragmentation reaction. A low-lying virtual  $s$ -state and a  $p$ -resonance are assumed in  $^{10}\text{Li}$  at 100 keV and 0.5 MeV, respectively. The  $p$ -wave content in  $^{10}\text{Li}$  is considered to be 4% (solid line), 18% (dashed line), and 32% (dot-dashed line).

We have now concluded that the asymmetries are sensitive essentially only to the non-zero angular momentum partial waves in the initial and final state wave function. Thus we also expect sensitivity to the content of the different waves in the two-body subsystem. In particular, for  $^{11}\text{Li}$  the asymmetries should depend on the  $p$ -wave content in  $^{10}\text{Li}$  subsystem (the neutron-neutron subsystem contains in any case almost exclusively  $s$ -waves). In Fig. 6 we show the same asymmetry,  $A_1^{3/2, 1/2}(p^{\parallel})$ , as in Fig. 4, but now assuming a virtual  $s$ -state at 100 keV and a  $p$ -resonance at 0.5 MeV in  $^{10}\text{Li}$ . By use of the spin-orbit parameter  $V_{so}^{l=1}$  in the neutron-core potential in Eq.(22) we modify the  $p$ -wave content in the neutron- $^9\text{Li}$  subsystem.

The solid line, dashed line, and dot-dashed line are the resulting calculations with 4%, 18%, and 32% of  $p$ -wave content in the  $^{10}\text{Li}$  wave function. In the three cases we observe the peak in the asymmetry around 30 MeV/c corresponding to the  $p$ -resonance at 0.5 MeV. The second peak in the asymmetry corresponds to the next  $p$ -resonance, closer to the first peak for a larger  $p$ -wave content, since the increase in the  $p$ -wave content is obtained by decreasing the energies of the  $p$ -resonances.

We observe that the lower the  $p$ -wave content the smaller the amplitudes of the oscillations of the asymmetry, see the solid line corresponding to the  $p$ -wave content of 4%. This is related to the fact that the asymmetry must vanish when the  $p$ -waves are totally absent. However, it should be mentioned that the denominator of the asymmetry in Eq.(18) is the unpolarized momentum distribution, that is known to be narrower for lower  $p$ -wave contents [19]. It is then possible to find oscillations with similar amplitude for different values of the  $p$ -wave content.

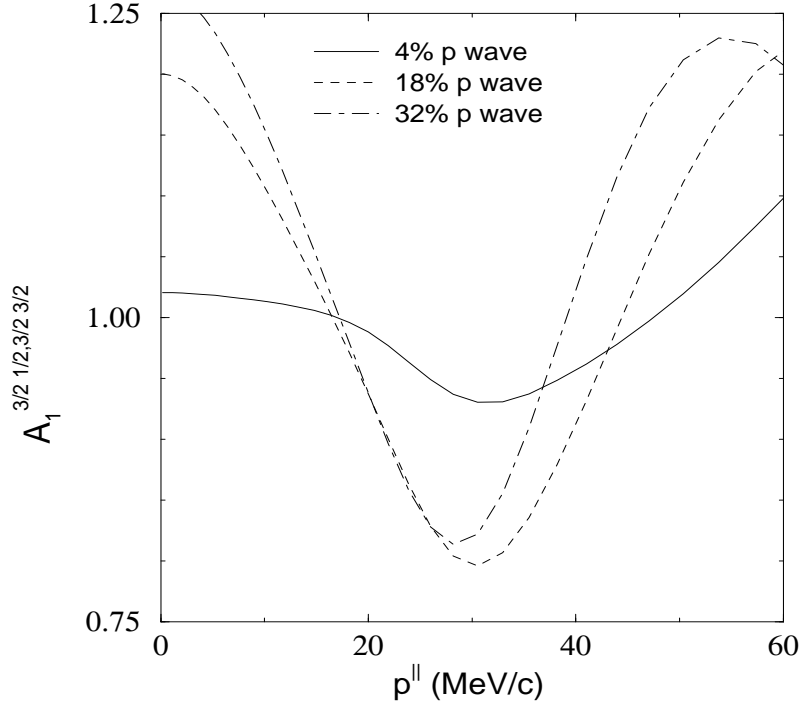


FIG. 7. The same as in Fig. 6 for the asymmetry  $A_1^{3/2 1/2; 3/2 3/2}(p^{\parallel})$ .

In Fig. 7 we show the same asymmetry,  $A_1^{3/2 1/2; 3/2 3/2}(p^{\parallel})$ , as in Fig. 6, i.e. one-dimensional neutron momentum distributions in a neutron removal reaction. As in Fig. 5 the spin projection of the core is assumed to be measured to have a value of  $3/2$  in the final state. Again, in this case the asymmetry shows essentially the same features as in Fig. 6, but with the advantage of larger amplitudes. The values of the asymmetries can vary now between 0.8 and more than 1.3.

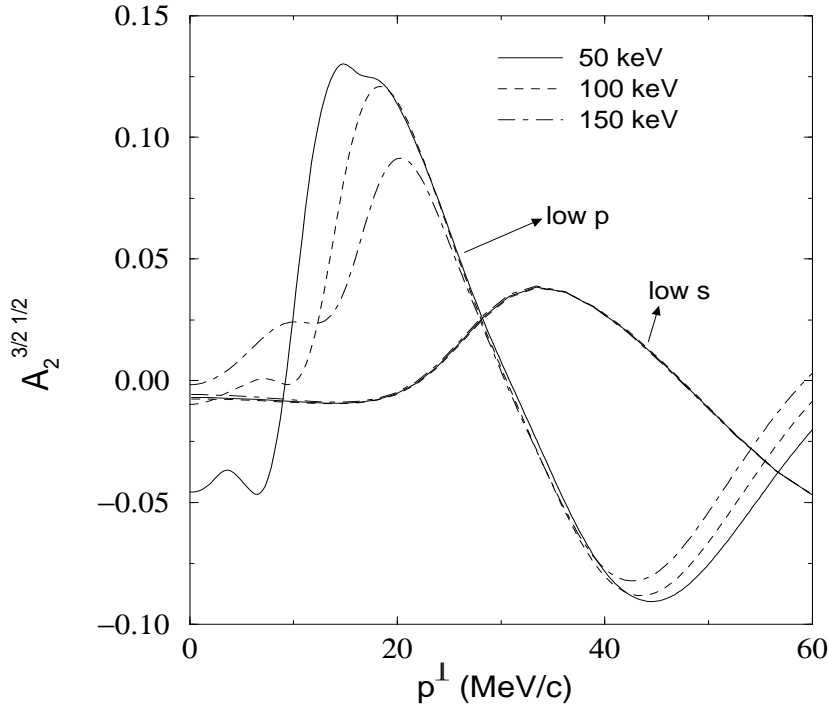


FIG. 8. The same as in Fig. 4 for the asymmetry  $A_2^{3/2 1/2}(p^{\perp})$ .

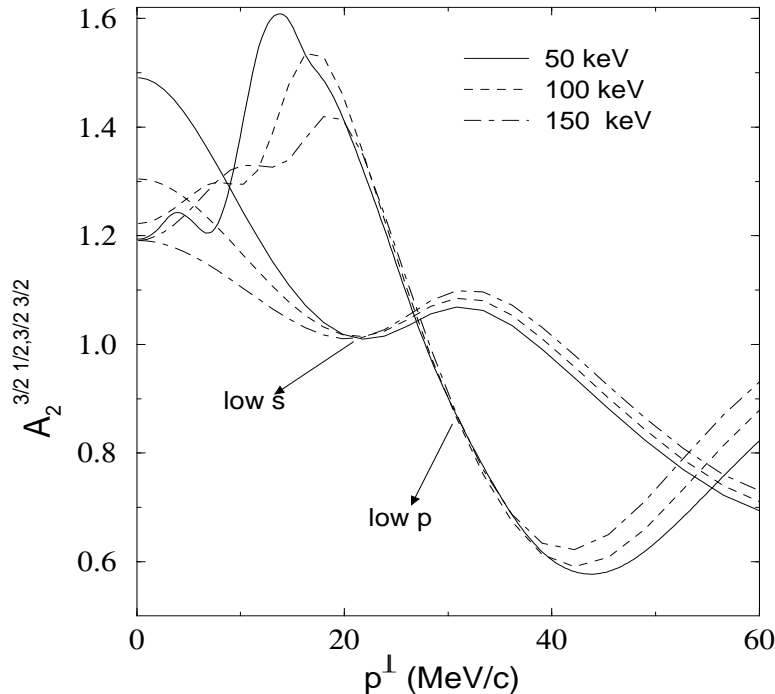


FIG. 9. The same as in Fig. 5 for the asymmetry  $A_2^{3/2 1/2; 3/2 3/2}(p^\perp)$ .

All the asymmetries we have discussed so far are obtained from one-dimensional neutron momentum distributions. The same conclusions can be obtained from the corresponding two-dimensional neutron momentum distributions shown for completeness in Figs. 8, 9, 10, 11. First we note that when only the beam is polarized the asymmetries are not sensitive to the structure of the virtual  $s$ -states in the two-body subsystems. When only the energy of the  $s$ -states is modified in the  $^{10}\text{Li}$  wave function the asymmetries do not change. Second, the minima and maxima of the asymmetries provide information about the  $p$ -resonance structure in the  $^{10}\text{Li}$  two-body subsystem. Third, the asymmetries are clearly dependent on the  $p$ -wave content of the  $^{10}\text{Li}$  wave function. Fourth, the asymmetries obtained assuming that the spin projection of the core has been measured in the final state ( $3/2$  in our case) show a clearly larger effect than those obtained assuming that only the beam is polarized.

In principle the same asymmetries could also be obtained from core momentum distributions and from neutron momentum distributions after core break-up. However these two cases are not especially interesting. The former because core momentum distributions are very little affected by the final state interaction, and then the asymmetries do not show very much structure. The latter because after core break-up the two neutrons survive in the final state, and the three-body wave function written in the Jacobi set where the  $\mathbf{x}$  coordinate is drawn between the two neutrons contains almost exclusively  $s$ -waves, to which the asymmetries are not sensitive.

#### IV. SUMMARY AND CONCLUSIONS

We have formulated a detailed model to investigate momentum distributions of particles emerging after nuclear break-up reactions of fast polarized three-body halo nuclei. The three main ingredients are:

(i) The three-body description of the initial nuclear wave function. This assumes that the particles or clusters are inert throughout the process and only distances larger than the cluster radii can be well described. Such models have been successfully applied to various light nuclei.

(ii) The sudden approximation where the target nucleus instantaneously removes one of the particles from the three-body projectile without disturbing the other two. This approximation is very well suited for short range interactions and fast processes where the beam velocity is much larger than the velocity of the intrinsic motion. The radioactive beams are available with high energies exceedingly well fulfilling this criterium.

(iii) The final state relative wave function for the two remaining particles must include effects of their mutual

interaction. The resulting distorted wave function may differ substantially from the plane wave solution when no two-body interaction is present. These effects are crucial when virtual s-states or higher angular momentum resonances occur at energies below about 1 MeV in the final state two-body system.

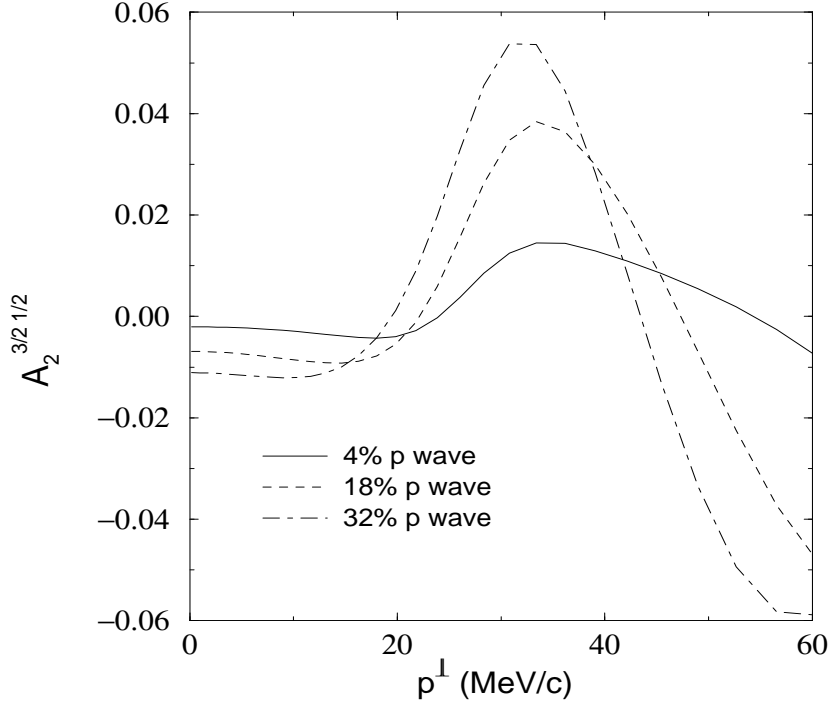


FIG. 10. The same as in Fig. 6 for the asymmetry  $A_2^{3/2 1/2}(p^\perp)$ .

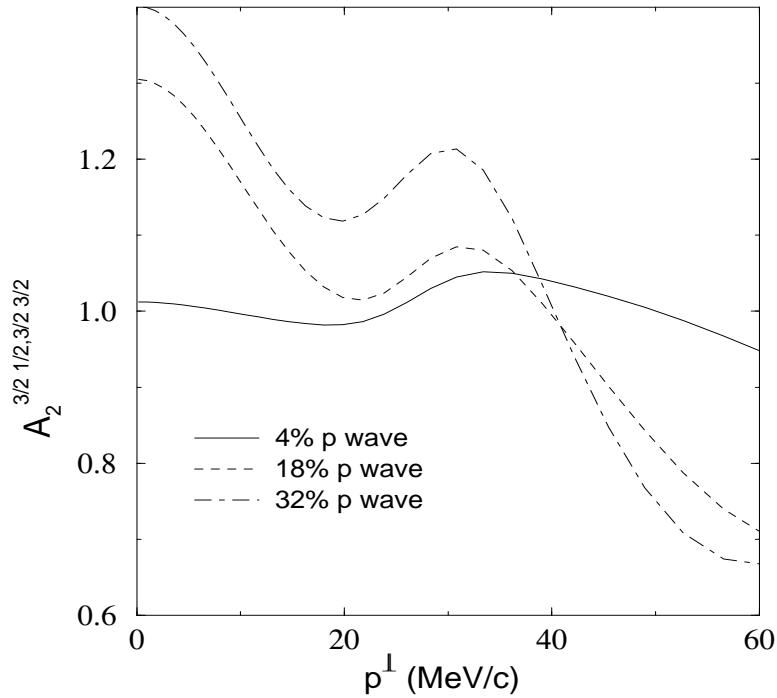


FIG. 11. The same as in Fig. 7 for the asymmetry  $A_2^{3/2 1/2; 3/2 3/2}(p^\perp)$ .

It is rather difficult to construct a theoretical system where assumption (i) is valid without the necessity of using (iii). The reason is that the three-body structure only is appropriate when the particles are fairly loosely bound, since they otherwise would overlap and destroy the cluster property. As a consequence the two-body subsystems must have fairly weak effective attractions yet they must be sufficiently strong to create a three-body bound state when working together. The result is low-lying continuum two-body structure.

The same two-body interactions are therefore responsible for both the initial three-body bound state and for the distorted final state wave function. A consistent treatment of initial and final stages of the process is therefore essential and our model meets this crucial requirement. In other words the two-body continuum structure is decisive for both the three-body halo structure and the momentum distributions after fragmentation.

We first describe the method to compute the momentum distributions in nuclear break-up processes. The overlap between initial and final state wave function is the essential quantity. The initial bound state three-body halo wave function is obtained by solving the Faddeev equations by use of an adiabatic hyperspherical expansion technique. This method has been tested previously and shown to be very efficient for ground states or low-lying excited states with small two-body relative orbital angular momenta. The final state distorted two-body continuum wave function is expanded in partial waves and the related radial wave functions are calculated numerically. They are normalized at large distances to coincide with the plane wave solutions. The resulting overlap matrix with different angular momentum projections is then available.

The cross sections or the observable momentum distributions are then essentially only the absolute square of the overlap integrated over unobserved quantities. These expressions contain numerically computed quantities. They appear to be rather complicated especially due to the use of the coordinate system where the center of mass of the three-body projectile is at rest and the dedicated goal of computing momentum distributions for polarized projectiles.

First we specify the two-body interactions appropriate for the  $^{11}\text{Li}$  system considered as two neutrons surrounding the  $^9\text{Li}$ -core. The neutron-neutron interaction is parametrized to reproduce low-energy scattering properties and then maintained throughout the present investigation. The neutron-core interaction is adjusted to reproduce the measured  $^{11}\text{Li}$  binding energy and root mean square radius. The remaining free parameters are used to place virtual s-states and p-resonances at various energies close to the threshold resulting in different  $^{11}\text{Li}$ -structures and different momentum distributions.

The final state two-body s-wave functions all have maxima at the origin. The highest value occurs when the scattering energy equals to the energy of the virtual s-state. The state is therefore peaked around zero and this localization is strongest around the energy of the virtual state. The p-state two-body wave function is peaked at an energy corresponding to the p-resonance energy. Without resonances and virtual states the wave functions are simply Bessel functions with the related oscillations and without these pronounced peak structures.

Neutron momentum distributions after neutron removal are computed for polarized  $^{11}\text{Li}$  and when the polarization of the final two-body state is measured. Several polarization observables are constructed and expressed in terms of quantities, called asymmetries, deviating from zero only when the momentum distributions depend on the polarization. Several continuum structures of  $^{10}\text{Li}$  are considered, but in all cases we maintain the binding energy and root mean square radius of  $^{11}\text{Li}$ .

The inclusion of the final state interaction is an essential ingredient in the computation, determining the behaviour of the asymmetries. In fact, when they are not included the structure in the polarization observables completely disappears. The core momentum distributions are little affected by the final state interaction, and therefore the asymmetries obtained from them exhibit very little structure.

From the asymmetries constructed from neutron momentum distributions we have observed the following features: If only the beam is polarized the asymmetries vanish when only s-waves contribute. This makes the asymmetries obtained from a core break-up reaction from  $^{11}\text{Li}$  not relevant, because almost exclusively s-waves are involved in this fragmentation process. Much more interesting are the asymmetries obtained from neutron momentum distributions after neutron removal reactions. The rest of the waves plays an important role, and the asymmetries become a perfect tool to investigate the  $\ell > 0$ -resonance structure of the neutron-core subsystem. These observables then contain information about the continuum structure of the two-body subsystems. In fact low-lying resonances (p-resonances in the  $^{11}\text{Li}$  case) in the neutron-core system show up as an extremum at the momentum value corresponding to the resonance energy. An additional measurement of the two-body final state polarization enhances the amplitudes of the asymmetries, but otherwise leaves essentially unchanged the structure of the asymmetry.

## APPENDIX A: RELATIVE MOMENTUM DISTRIBUTIONS

In this appendix we give the analytic expressions for the relative momentum distributions of the two particles in the final state. We consider three different cases:

(i) 100% polarized beam and spin projection of one of the particles in the final state measured:

$$\begin{aligned}
\frac{d^3\sigma}{dk_y dk_x^\perp dk_x^\parallel} &\propto k_y^2 k_x^\perp \frac{2}{\pi^2} \sum_{I L_x} (-1)^{J-M} \hat{I}^2 \begin{pmatrix} J & J & I \\ M & -M & 0 \end{pmatrix} P_{L_x}(\cos \theta_{k_x}) \\
&\sum_{j_x \ell_x s_x j'_x \ell'_x s'_x} \sum_{L S L' S'} \sum_{\ell_y j_y} (-1)^{\ell_x + J - s'_x + 2s_y - j_y + j_x - s_2 - s_1} \hat{j}_x^2 \hat{j}_x^2 \hat{j}_y^2 \hat{J}^2 \hat{\ell}_x \hat{\ell}'_x \hat{L} \hat{L}' \hat{S} \hat{S}' \hat{s}_x \hat{s}'_x \hat{L}_x^2 \hat{s}_1^2 \\
&I_{\ell_x s_x j_x}^{\ell_y L S}(\kappa, \alpha_\kappa) I_{\ell'_x s'_x j'_x}^{\ell'_y L' S'}(\kappa, \alpha_\kappa) \begin{Bmatrix} J & j_x & j_y \\ L & \ell_x & \ell_y \\ S & s_x & s_y \end{Bmatrix} \begin{Bmatrix} J & j'_x & j_y \\ L' & \ell'_x & \ell_y \\ S' & s'_x & s_y \end{Bmatrix} \begin{Bmatrix} j_x & j'_x & I \\ J & J & j_y \end{Bmatrix} \begin{pmatrix} \ell_x & \ell'_x & L_x \\ 0 & 0 & 0 \end{pmatrix} \\
&\sum_{I'} (-1)^{I' + s_1 - \sigma_1} \hat{I}'^2 \begin{pmatrix} s_1 & s_1 & I' \\ \sigma_1 & -\sigma_1 & 0 \end{pmatrix} \begin{pmatrix} I' & I & L_x \\ 0 & 0 & 0 \end{pmatrix} \begin{Bmatrix} s_1 & I' & s_1 \\ s'_x & s_2 & s_x \end{Bmatrix} \begin{Bmatrix} s_x & s'_x & I' \\ j_x & j'_x & I \\ \ell_x & \ell'_x & L_x \end{Bmatrix} \quad (A1)
\end{aligned}$$

(ii) 100% polarized beam and no spins projections measured in the final state:

This amounts to multiply the previous expression by  $1/(2s_1 + 1)$  and sum over  $\sigma_1$ . The main consequence of the summation is that the index  $I'$  is zero, and then  $L_x = I$ . Then we get the expression

$$\begin{aligned}
\frac{d^3\sigma}{dk_y dk_x^\perp dk_x^\parallel} &\propto k_y^2 k_x^\perp \frac{2}{\pi^2} \sum_I (-1)^{J-M} \hat{I}^2 \begin{pmatrix} J & J & I \\ M & -M & 0 \end{pmatrix} P_I(\cos \theta_{k_x}) \quad (A2) \\
&\sum_{j_x \ell_x s_x j'_x \ell'_x} \sum_{L S L' S'} \sum_{\ell_y j_y} (-1)^{2s_y + J - s_x + j_x - j'_x - j_y} \hat{j}_x^2 \hat{j}_x^2 \hat{j}_y^2 \hat{J}^2 \hat{\ell}_x \hat{\ell}'_x \hat{L} \hat{L}' \hat{S} \hat{S}' I_{\ell_x s_x j_x}^{\ell_y L S}(\kappa, \alpha_\kappa) \\
&I_{\ell'_x s'_x j'_x}^{\ell'_y L' S'}(\kappa, \alpha_\kappa) \begin{Bmatrix} J & j_x & j_y \\ L & \ell_x & \ell_y \\ S & s_x & s_y \end{Bmatrix} \begin{Bmatrix} J & j'_x & j_y \\ L' & \ell'_x & \ell_y \\ S' & s'_x & s_y \end{Bmatrix} \begin{pmatrix} \ell_x & \ell'_x & I \\ 0 & 0 & 0 \end{pmatrix} \begin{Bmatrix} j_x & j'_x & I \\ J & J & j_y \end{Bmatrix} \begin{Bmatrix} j_x & j'_x & I \\ \ell'_x & \ell_x & s_x \end{Bmatrix}
\end{aligned}$$

(iii) Unpolarized beam and no spins projections measured in the final state:

Multiplying by  $1/(2J + 1)$  and summing over  $M$  we get the totally unpolarized momentum distribution. From the summation we obtain that  $I = 0$ , and the analytic expression is

$$\begin{aligned}
\frac{d^3\sigma}{dk_y dk_x^\perp dk_x^\parallel} &\propto k_y^2 k_x^\perp \frac{2}{\pi^2} \sum_{j_x \ell_x s_x} \sum_{L S L' S'} \sum_{\ell_y j_y} \hat{j}_x^2 \hat{j}_x^2 \hat{L} \hat{L}' \hat{S} \hat{S}' I_{\ell_x s_x j_x}^{\ell_y L S}(\kappa, \alpha_\kappa) I_{\ell_x s_x j_x}^{\ell_y L' S'}(\kappa, \alpha_\kappa) \\
&\begin{Bmatrix} J & j_x & j_y \\ L & \ell_x & \ell_y \\ S & s_x & s_y \end{Bmatrix} \begin{Bmatrix} J & j_x & j_y \\ L' & \ell_x & \ell_y \\ S' & s_x & s_y \end{Bmatrix} \quad (A3)
\end{aligned}$$

## APPENDIX B: MOMENTUM DISTRIBUTIONS RELATIVE TO THE CENTER OF MASS OF THE PROJECTILE

In this appendix we give the analytic expressions for the momentum distributions of the two particles in the final state relative to the center of mass of the incident three-body system. The same three cases as in the previous appendix are considered:

(i) 100% polarized beam and spin projection of one of the particles in the final state measured:

$$\begin{aligned}
\frac{d^4\sigma}{dk_y d\theta'_{k_y} dp^\perp dp^\parallel} &\propto \sin \theta'_{k_y} k_y^2 p^\perp \frac{1}{a_i^3 \pi^2} \sum_I (-1)^{J-M} \hat{I}^2 \begin{pmatrix} J & J & I \\ M & -M & 0 \end{pmatrix} \sum_{\ell_x s_x j_x L S} \\
&\sum_{\ell'_x s'_x j'_x L' S'} \sum_{\ell_y j_y \ell'_y j'_y} (-1)^{s_y - \ell_x + 2j'_x + j'_y - s_2 - s_1 + s'_x} \hat{j}_x^2 \hat{j}_x^2 \hat{j}_y^2 \hat{j}_y^2 \hat{J}^2 \hat{\ell}_x \hat{\ell}'_x \hat{\ell}_y \hat{\ell}'_y \hat{L} \hat{L}' \hat{S} \hat{S}' \\
&\hat{s}_x \hat{s}'_x \hat{s}_1^2 I_{\ell_x s_x j_x}^{\ell_y L S}(\kappa, \alpha_\kappa) I_{\ell'_x s'_x j'_x}^{\ell'_y L' S'}(\kappa, \alpha_\kappa) \begin{Bmatrix} J & j_x & j_y \\ L & \ell_x & \ell_y \\ S & s_x & s_y \end{Bmatrix} \begin{Bmatrix} J & j'_x & j'_y \\ L' & \ell'_x & \ell'_y \\ S' & s'_x & s'_y \end{Bmatrix} \sum_{L_x L_y} \hat{L}_x^2 \hat{L}_y^2 \\
&\begin{pmatrix} \ell_x & \ell'_x & L_x \\ 0 & 0 & 0 \end{pmatrix} \begin{pmatrix} \ell_y & \ell'_y & L_y \\ 0 & 0 & 0 \end{pmatrix} \begin{Bmatrix} j_y & j'_y & L_y \\ \ell'_y & \ell_y & s_y \end{Bmatrix} \sum_{T N_x} \hat{T}^2 (-1)^T P_T(\cos \theta_p)
\end{aligned}$$



$$\begin{aligned}
& \begin{pmatrix} L_x & L_y & T \\ N_x & -N_x & 0 \end{pmatrix} \sqrt{\frac{(L_x - N_x)!(L_y + N_x)!}{(L_x + N_x)!(L_y - N_x)!}} P_{L_x}^{N_x}(\cos \theta'_{k_x}) P_{L_y}^{-N_x}(\cos \theta'_{k_y}) \\
& \sum_{I'I''} (-1)^{s_1 - \sigma_1 + I' - I''} \hat{I}'^2 \hat{I}''^2 \begin{pmatrix} s_1 & s_1 & I' \\ \sigma_1 & -\sigma_1 & 0 \end{pmatrix} \begin{Bmatrix} j_x & j'_x & I'' \\ j_y & j'_y & L_y \\ J & J & I \end{Bmatrix} \begin{Bmatrix} s_x & s'_x & I' \\ j_x & j'_x & I'' \\ \ell_x & \ell'_x & L_x \end{Bmatrix} \\
& \begin{Bmatrix} s_1 & I' & s_1 \\ s'_x & s_2 & s_x \end{Bmatrix} \begin{pmatrix} I & T & I' \\ 0 & 0 & 0 \end{pmatrix} \begin{Bmatrix} I & T & I' \\ L_x & I'' & L_y \end{Bmatrix}
\end{aligned} \tag{B1}$$

(ii) 100% polarized beam and no spins projections measured in the final state:

$$\begin{aligned}
& \frac{d^4 \sigma}{dk_y d\theta'_{k_y} dp^\perp dp^\parallel} \propto \sin \theta'_{k_y} k_y^2 p^\perp \frac{1}{a_i^3 \pi^2} \sum_I (-1)^{J-M} \hat{I}^2 P_I(\cos \theta_p) \begin{pmatrix} J & J & I \\ M & -M & 0 \end{pmatrix} \\
& \sum_{\ell_x s_x j_x L S} \sum_{\ell'_x j'_x L' S'} \sum_{\ell_y j_y \ell'_y j'_y} (-1)^{s_y + j'_x + j'_y + s_x + I} \hat{j}_x^2 \hat{j}_x^2 \hat{j}_y^2 \hat{j}_y^2 \hat{J}^2 \hat{\ell}_x \hat{\ell}_x \hat{\ell}_y \hat{\ell}_y \hat{L} \hat{L}' \hat{S} \hat{S}' \\
& I_{\ell_x s_x j_x L S}^{\ell_y L S}(\kappa, \alpha_\kappa) I_{\ell'_x j'_x L' S'}^{\ell'_y L' S'}(\kappa, \alpha_\kappa) \begin{Bmatrix} J & j_x & j_y \\ L & \ell_x & \ell_y \\ S & s_x & s_y \end{Bmatrix} \begin{Bmatrix} J & j'_x & j'_y \\ L' & \ell'_x & \ell'_y \\ S' & s_x & s_y \end{Bmatrix} \sum_{L_x L_y} (-1)^{L_x + L_y} \hat{L}_x^2 \hat{L}_y^2 \\
& \begin{pmatrix} \ell_x & \ell'_x & L_x \\ 0 & 0 & 0 \end{pmatrix} \begin{pmatrix} \ell_y & \ell'_y & L_y \\ 0 & 0 & 0 \end{pmatrix} \begin{Bmatrix} j_y & j'_y & L_y \\ \ell'_y & \ell_y & s_y \end{Bmatrix} \begin{Bmatrix} j_x & j'_x & L_x \\ j_y & j'_y & L_y \\ J & J & I \end{Bmatrix} \begin{Bmatrix} j_x & j'_x & L_x \\ \ell'_x & \ell_x & s_x \end{Bmatrix} \\
& \sum_{N_x} \begin{pmatrix} L_x & L_y & I \\ N_x & -N_x & 0 \end{pmatrix} \sqrt{\frac{(L_x - N_x)!(L_y + N_x)!}{(L_x + N_x)!(L_y - N_x)!}} P_{L_x}^{N_x}(\cos \theta'_{k_x}) P_{L_y}^{-N_x}(\cos \theta'_{k_y})
\end{aligned} \tag{B2}$$

(iii) Unpolarized beam and no spins projections measured in the final state:

$$\begin{aligned}
& \frac{d^4 \sigma}{dk_y d\theta'_{k_y} dp^\perp dp^\parallel} \propto \sin \theta'_{k_y} k_y^2 p^\perp \frac{1}{a_i^3 \pi^2} \sum_{\ell_x s_x j_x L S} \sum_{\ell'_x j'_x L' S'} \sum_{\ell_y j_y \ell'_y j'_y} (-1)^{s_y - s_x + j'_y + j_y + J} \\
& \hat{j}_x^2 \hat{j}_x^2 \hat{j}_y^2 \hat{j}_y^2 \hat{\ell}_x \hat{\ell}_x \hat{\ell}_y \hat{\ell}_y \hat{L} \hat{L}' \hat{S} \hat{S}' I_{\ell_x s_x j_x L S}^{\ell_y L S}(\kappa, \alpha_\kappa) I_{\ell'_x s_x j'_x L' S'}^{\ell'_y L' S'}(\kappa, \alpha_\kappa) \begin{Bmatrix} J & j_x & j_y \\ L & \ell_x & \ell_y \\ S & s_x & s_y \end{Bmatrix} \\
& \begin{Bmatrix} J & j'_x & j'_y \\ L' & \ell'_x & \ell'_y \\ S' & s_x & s_y \end{Bmatrix} \sum_{L_x} \hat{L}_x^2 \begin{pmatrix} \ell_x & \ell'_x & L_x \\ 0 & 0 & 0 \end{pmatrix} \begin{pmatrix} \ell_y & \ell'_y & L_y \\ 0 & 0 & 0 \end{pmatrix} \begin{Bmatrix} j_y & j'_y & L_x \\ \ell'_y & \ell_y & s_y \end{Bmatrix} \begin{Bmatrix} j_x & j'_x & L_x \\ \ell'_x & \ell_x & s_x \end{Bmatrix} \\
& \begin{Bmatrix} j_x & j'_x & L_x \\ j'_y & j_y & J \end{Bmatrix} \sum_{N_x} (-1)^{N_x} P_{L_x}^{N_x}(\cos \theta'_{k_x}) P_{L_x}^{-N_x}(\cos \theta'_{k_y})
\end{aligned} \tag{B3}$$

All the three previous expressions are valid when  $a < 0$ . For  $a > 0$  the summation over  $N_x$  should include an extra factor  $(-1)^{N_x}$ .

If we assume that one of the particles in the final state, say particle 1, has infinite mass, then the momentum distribution of particle 2 relative to the three-body center of mass should coincide with the momentum distribution relative to particle 1. In other words, Eqs.(A1), (A2), and (A3) should be recovered by integrating over  $\theta'_{k_y}$ . Eqs.(B1), (B2), and (B3), respectively. In this case  $b_i = 0$ , see Eq.(16),  $\mathbf{p} = a_i \mathbf{k}_x$  and therefore  $\theta'_{k_x} = 0$  and  $P_{L_x}^{N_x}(1) = \delta_{N_x, 0}$ . Now  $\kappa$  and  $\alpha_\kappa$  are independent of  $\theta'_{k_y}$ , and the integration over  $\theta'_{k_y}$  can easily be done analytically leading directly to Eqs.(A1), (A2), and (A3).

**Acknowledgments.** One of us (E.G.) acknowledges support from the European Union through the Human Capital and Mobility program contract nr. ERBCHBGCT930320.

- [2] C. Bertulani, L.F. Canto, and M.S. Hussein, Phys. Rep. 226 (1993) 281
- [3] P.G. Hansen, A.S. Jensen, and B. Jonson, Annu. Rev. Nucl. Part. Sci. 45 (1995) 591
- [4] P.G. Hansen and B. Jonson, Europhys. Lett. 4 (1987) 409
- [5] L. Johannsen, A.S. Jensen, and P.G. Hansen, Phys. Lett. B244 (1990) 357
- [6] D.V. Fedorov, A.S. Jensen, and K. Riisager, Phys. Rev. C49 (1994) 201
- [7] T. Kobayashi, O. Yamakawa, K. Omata, K. Sugimoto, T. Shimoda, N. Takahashi and Tanihata, Phys. Rev. Lett. 60 (1988) 2599
- [8] R. Anne *et al.*, Phys. Lett. B250 (1990) 19
- [9] N.A. Orr *et al.*, Phys. Rev. Lett. 69 (1992) 2050
- [10] N.A. Orr *et al.*, Phys. Rev. C51 (1995) 3116
- [11] M. Zinser *et al.*, Phys. Rev. Lett. 75 (1995) 1719
- [12] T. Nilsson *et al.*, Europhys. Lett. 30 (1995) 19
- [13] F. Humbert *et al.*, Phys. Lett. B347 (1995) 198
- [14] M.V. Zhukov, L.V.Chulkov, D.V. Fedorov, B.V. Danilin, J.M. Bang, J.S. Vaagen and I.J. Thompson, J. Phys. G20 (1994) 201
- [15] A.A. Korshennikov and T. Kobayashi, Nucl. Phys. A567 (1994) 97
- [16] I.J. Thompson and M.V. Zhukov, Phys. Rev. C49 (1994)1904
- [17] M.V. Zhukov and B. Jonson, Nucl. Phys. A589 (1995) 1
- [18] , F. Barranco, E. Vigezzi, and R.A. Broglia, Phys. Lett. B319 (1993) 387
- [19] E. Garrido, D.V. Fedorov and A.S. Jensen, Phys. Rev. C53 (1996) 3159, and submitted for publication
- [20] D.V. Fedorov, A.S. Jensen, and K. Riisager, Phys. Rev. C50 (1994) 2372
- [21] E. Garrido, D.V. Fedorov and A.S. Jensen, Phys. Rev. C51 (1995) 3052
- [22] A. Cobis, D.V. Fedorov, and A.S. Jensen, submitted for publication
- [23] R.G. Newton, Scattering Theory of Waves and Particles, Second Edition (Springer-Verlag, New York, 1982), p.444
- [24] B.M. Young *et al.*, Phys. Rev. Lett. 71 (1993) 4124
- [25] I. Tanihata *et al.*, Phys. Lett. B287 (1992) 307
- [26] B.M. Young *et al.*, Phys. Rev. C49 (1994) 279
- [27] R.A. Kryger *et al.*, Phys. Rev. C47 (1993) R2439
- [28] H.G. Bohlen *et al.*, Z. Phys. A344 (1993) 381